WiChronos : Energy-Efficient Modulation for Long-Range, Large-Scale Wireless Networks

Yaman Sangar
University of Wisconsin-Madison
sangar@wisc.edu

Bhuvana Krishnaswamy
University of Wisconsin-Madison
bhuvana@ece.wisc.edu

ABSTRACT

Wireless communication over long distances has become the bottleneck for battery-powered, large-scale deployments. Currently used low-power protocols such as Zigbee and Bluetooth Low Energy have limited communication range, whereas long-range communication strategies used in cellular and satellite networks are heavy on energy consumption. Methods that use narrow-band communication such as LoRa, SigFox, and NB-IoT have low spectral efficiency, leading to scalability issues. The goal of this work is to develop a communication framework that can satisfy the following requirements: (1) Increased battery life, (2) Longer communication range, (3) Scalability in a wireless network. In this work, we propose, design, and prototype WiChronos, a communication paradigm that encodes information in the time interval between two narrowband symbols in order to drastically reduce the energy consumption in a wide area network with a large number of senders. We leverage the low data-rate and relaxed latency requirements of such applications to achieve the desired features identified above. Based on our prototype using off-the-shelf components, WiChronos achieves an impressive 60% improvement in battery life compared to state-of-the-art LPWAN technologies at distances of over 800 meters. We also show that more than 1000 WiChronos senders can co-exist with less than 5% probability of collisions under low traffic conditions.

1 INTRODUCTION

Wireless data delivery is key to real-time data collection and analysis in the fast-growing areas of smart agriculture [1, 2], livestock monitoring [3], and precision farming [4]. Large-scale soil monitoring networks currently use cellular and satellite networks to collect real-time data over a long period of time [5]. Real-time data collection from in-situ sensors in fields throughout the crop season will provide an understanding of the spatio-temporal dynamics of environmental factors and various chemical and biological

processes in the soil, which can, in turn, be used to improve soil health and crop growth. However, due to the high infrastructure costs for solar panels and batteries to enable wireless information retrieval, monitoring sensor networks are deployed only at limited locations and have latencies ranging from one day up to one month [5, 6]. Such monitoring systems typically deploy sensors in large fields and share the following requirements: (1) Long battery life, (2) Long-range communication to reduce infrastructure costs, (3) Scalability and co-existence, (4) Low cost, with less stringent demands on data rate, latency, and payload size compared to traditional networks For example, sensors used to measure soil moisture, the chemical and biological properties of soil typically have a resolution of 8-12 bits [7–9], offering a light payload. Also, the gradual change in the rate of these parameters results in reduced demands for data-rate and latency. However, the monitoring systems are often deployed in harsh, remote environments on a massive scale and are expected to have battery life in the order of years.

Current energy-efficient protocols such as Zigbee [10], blacktooth Low Energy (BLE) [11], and backscattering [12–15] consume less than 50mW power during active transmission, allowing for a long battery life. However, their communication range is on the order of 10s of meters, and they require infrastructure support for coverage. On the other hand, approaches for long range such as cellular and satellite networks are expensive and energy consuming, limiting the battery life and scalability of the system. In Table 1, we compare the battery-life, communication range, scalability, and achievable data-rate of existing wireless technologies. *Evidently, existing strategies for addressing low-power and long-range do not co-exist efficiently in a large-scale network.* This inefficiency can be explained by the impact of bandwidth (BW) on energy consumption, communication range, and network capacity. In an additive white Gaussian noise channel, the maximum channel data-rate is given by,

$$C = B \, \log_2 \left(1 + \frac{S}{N_0 B} \right), \tag{1}$$

where B is the signal BW in Hz, S is the signal power and N_0 is the noise spectral density [16]. A wideband signal can achieve a high data rate, in-turn reducing the time-on-air (the amount of time a channel is occupied). With reduced time-on-air, the active transmit time of the RF module decreases, in-turn reducing energy consumption. However, the signal-to-noise ratio (SNR), $\frac{S}{N_0 B}$, decreases with an increase in BW, since the noise power increases with BW. At long distances, the received signal power decreases due to path loss; hence a lower BW can decrease noise power and increase the SNR. Therefore, a narrowband (NB) signal is more suitable for propagation over long distances with an acceptable SNR.

$$\text{Energy} \propto \text{Time-on-air} \propto \frac{1}{B}, \quad \text{Range} \propto \frac{1}{B}, \quad \text{Scale} \propto B.$$

	Battery Life (> 1 yr)	Range (> 1 km)	Scalable (> 1000)	Data-rate (kbps)
WiFi	X	X	X	<54k
Cellular	X	X	✓	<10k
BLE	✓	X	X	<2k
Zigbee	✓	X	X	<250
Passive RFID [17]	✓	X	X	<40
Active RFID [18]	✓	X	X	<40
AmbientBackscatter [13]	✓	X	X	<1
LoRaBackscatter [15]	✓	✓	X	<37.5
pLoRa [14]	✓	✓	X	<.0002
LoRa	✓	✓	X	<27
SigFox	✓	✓	X	<.6
WiChronos	✓	✓	✓	<1

**Table 1: Comparison of current wireless technologies and WiChronos**

This conflicting requirement on bandwidth makes it challenging for low-power and long-range solutions to co-exist.

LPWAN (Low Power Wide Area Network) technologies such as LoRa [19], SigFox [20], NB-IoT [21] have been successful in achieving long range [22, 23] and long battery life by limiting the *duty-cycle* (the fraction of time during which a node is in active transmit or receive mode) by reducing the number of messages per day. In other words, existing LPWAN solutions reduce the overall energy by limiting the airtime of each device in a day. They do not address the fundamental tradeoff between low-power and long-range. Therefore, as the network scales, their cumulative airtime will increase, leading to an increase in the probability of collisions, rendering them unsuitable for large-scale deployment.

In this work, we develop a communication framework that addresses the fundamental trade-off between low power and long range in large-scale networks that have relaxed data-rate and latency requirements. *We propose WiChronos, a modulation technique that encodes information in the time interval between two narrowband symbols.* A WiChronos sender transmits exactly two *anchor* symbols per message, namely *preamble* and *postamble*, and the data modulates the duration between them. We leverage the low data rate and small payload requirements of monitoring systems in agriculture, remote tracking, and derive benefits from the availability of resources at the receiver to make transmitters energy efficient.

WiChronos achieves **energy efficiency** by minimizing the number of symbols and (hence the time-on-air) per message, and **long range** by transmitting the anchor symbols over ultra-narrowband (UNB) [24]. The reduced time-on-air and improved spectral efficiency allow the network to **scale better**. WiChronos trades off data-rate to achieve the above three features.

Fig. 1 illustrates WiChronos and contrasts it with existing modulations. A WiChronos sender with a sensor data of 678 units transmits an anchor symbol (*preamble*), goes to sleep for 678 clock cycles (that corresponds to data), and wakes up to send another anchor symbol (*postamble*). The anchor symbols consist of a training sequence of alternating 0s and 1s followed by a unique sender address. The sleep time encodes the entire message to be transmitted. The time-on-air of WiChronos is thus independent of the payload length (10 bits in this example) and only a function of the anchor symbols; by separating payload transmission from time-on-air, we reduce
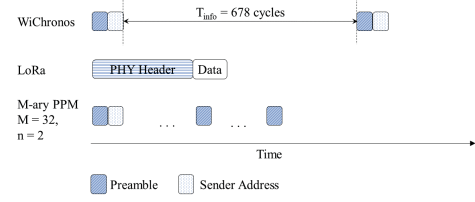
Fig. 1: WiChronos illustration

the impact of BW on the time-on-air, without affecting the communication range. In the case of traditional modulations such as LoRa or SigFox, the data value of 678 is mapped to bits, which are then mapped to symbols for the corresponding modulation technique and transmitted over the air and hence the time-on-air is proportional to the payload length. Other time interval based modulations such as M-PPM transmit multiple pulses over air; the time slots in which the pulses are sent indicate the message. In order to achieve a higher datarate, lower latency, and reduce clock skew errors due to imperfect slot synchronization, the number of slots per frame is typically set low. Therefore, the number of pulses is high for longer payloads, in turn increasing the time-on-air.

Towards implementing WiChronos in a wireless network, we identify the challenges in designing an optimal anchor symbol in terms of length, modulation parameters, and medium access control (MAC) in §4. We prototype WiChronos using inexpensive off-the-shelf radio modules and microcontroller units (MCU), using software-only changes. Based on our experimental implementation on MSP 430 [25] and Linx-NT [26], we achieved an impressive battery life of over 5 years using a coin cell battery (250mAh) at a range close to 1 km. Also, we estimate the probability of collision to be less than 5% in a 1000 node network under low traffic conditions. To this end, we make the following contributions:

- We propose an energy-efficient modulation technique that encodes information in the time interval between two symbols, minimizing the number of symbols per message.
- We propose a spectrally-efficient physical layer design with UNB anchor symbols, improving the receiver sensitivity and range.
- We implement an ALOHA-based MAC protocol and analyze its robustness to collisions in large-scale deployments, allowing the network to scale seamlessly.
- We prototype the proposed framework using off-the-shelf, low-cost RF modules and MCUs with low-power clocks.

The remainder of this paper is organized as follows. In §2, we provide background on the strategies for low power and long range, and motivate the need for a unifying algorithm in a large-scale network. In §4, we present the design and features of WiChronos, followed by a discussion on the challenges and throughput performance in §5. Experimental evaluation is presented in §6. Related work is discussed in §3, followed by discussions and future work in §7. Finally, §8 concludes the paper.

2 BACKGROUND AND MOTIVATION

The overall power consumed by a sensor node is dominated by the communication module [27, 28]. Algorithms, protocols, and architectures have been developed to reduce the active transmit time and hence reduce the power consumption in the areas of

Wireless Sensor Networks (WSN), AdHoc Networks, and Internet-of-Things. We broadly classify existing low power strategies for WSNs into the following five categories [4, 29–31]: (1) Duty Cycling, (2) Routing, (3) Data reduction, (4) Radio module optimization, (5) Energy harvesting and backscatter.

Smart sleep/wake-up protocols [32, 33], event-triggered wake-up [34], and scheduled MAC protocols [35, 36] have been proposed to reduce the active transmit and/or receive time of the radio transceiver. Though duty-cycling-based approaches reduce the power consumption of the overall network, they are still limited by the payload length. Data compression [37], prediction [38, 39], and cooperative communication [40, 41] techniques have been proposed to reduce the amount of data to be transmitted, which in turn reduces the energy per message. Network topology aware strategies have been developed to improve the lifetime of a sensor network through clustering [42], energy-aware routing [43], data gathering, and data forwarding [44]. These approaches decrease the overall energy consumption of the network by leveraging the hierarchical topology and varying the energy constraints of nodes in the network [45, 46]. A new wave of battery-less sensors harvest energy from ambient signals and/or dedicated sources [13, 15] and use backscattering to communicate. However, these techniques are feasible only within a short range and require an additional signal source to piggyback on for long-range communication [14, 15]. Active and passive RFID tags [17, 18] are energy efficient but only work for a short range [47] and/or low traffic. RFIDs also are limited by the energy-range-scale tradeoff presented in §1.

As discussed in §1, the limited range of existing energy-efficient strategies can be attributed to the BW and propagation of radio frequency (RF) signals. The range of an RF signal depends on the link budget that accounts for the gains and the losses.

$$P_{Rx} = P_{Tx} + P_G - P_L, \qquad (2)$$

where P_{Rx} is the received power, P_{Tx} is the transmit power, P_G is the antenna gains of the system, and P_L is the aggregate loss due to filter/cable attenuation, known experimental conditions, and path loss (P_{PL}). Free space path loss is given by

$$P_{PL} = -10 \log_{10} \frac{\lambda^2}{(4\pi d)^2} = 22dBm + 20 \log_{10} \frac{d}{\lambda}, \qquad (3)$$

where d is the distance between the sender and the receiver, and λ the wavelength. Radio optimization techniques to improve P_{Tx} such as directional antennas [35], Multiple-Input Multiple-Output, and mobility-based solutions such as Mobile Ad-Hoc Networks [48–50] are energy consuming and not suitable for low-power communication. Given the FCC limit on transmit power, the link budget depends on the path loss, which is inversely proportional to the wavelength (i.e., path loss increases with increasing frequency).

Existing technologies for long-range such as cellular networks, NB-IoT, Sigfox, and LoRa operate in the sub-GHz bands to reduce path loss. Cellular and NB-IoT require high-complexity RF front-end and LTE infrastructure for scheduling and synchronization [51].

SigFox and LoRa operate at lower BW to achieve long range, leading to an increase in the time-on-air. Similarly, Zigbee 3.0 [52] reduces datarate and increases transmit power to improve range inturn increasing time-on-air. To achieve long battery life, LPWAN solutions limit the number of messages per day. Therefore, as the number of messages increases, the overall energy consumption increases, making them inefficient for an energy-constrained system. Also, with increasing scale, collision rate increases, which leads to a decrease in the network throughput [19–21].

To summarize, existing energy-efficient and long-range strategies cannot co-exist in a large-scale network. In this work, we develop a communication framework for real-time monitoring system that is energy-efficient, communicates over long distances, and supports a large number of nodes.

3 RELATED WORK

Timing interval based communication has been studied in the past. We present an overview of these works below.

Information Theoretic Analysis : An information theoretic analysis of encoding information in the queuing time has been studied in literature [53–57]. While bounds on channel capacity of single-queue and multiple-queue servers worst-case timing error distributions have been studied, they do not provide algorithms for energy efficiency and/or long-range communication in a wireless system. The maximum achievable data-rate of WiChronos aligns with the capacity of timing channel derived in [53].

Timing Channel: Timing based communication has been studied as a security risk in covert timing channels [58–60], where information is encoded covertly in the time interval. The majority of the research work on timing channels has focused on defense mechanisms to eliminate timing channels.

Pulse Time Modulation: This work is motivated by Pulse Position Modulation (PPM) and Communication through Silence [61], a challenges paper on timing based modulation in wireless sensor networks. [61] does not consider long-range and scalability in wireless networks. It does not consider the challenges in the practical implementation of timing interval modulation in wireless networks such as anchor symbol length, synchronization, and packet errors. To the best of our knowledge, WiChronos is the first attempt at implementing timing interval modulation technique for long-range, energy efficient communication in wireless networks.

PPM and its variants such as Differential PPM [62, 63], M-ary PPM [64–68] have been developed and widely used in one-to-one optical networks with ultra wide bandwidth and narrow pulses. The following requirements of typical PPM implementations make them challenging for wireless networks.

Bandwidth requirements: PPM and its variants typically use an ultra-wide bandwidth [64] to get a narrow pulse to achieve reasonable data rates while also saving energy. Ultra wide band will result in an increase in energy consumption and noise floor in a wireless module, affecting both battery life and range. To overcome this challenge, we use narrow bandwidth and achieve long range.

Clock Synchronization: In UWB, the pulses are short and therefore symbol synchronization is required for PPM. DPPM, however, overcomes this challenge by encoding in the time difference between pulses [62]. In this work, we relax synchronization requirements with the help of differential modulation and low data-rates. PPM implemented in one-to-one optical links does not require a dedicated MAC protocol. However, in a wireless network, the pulses collide on air and therefore dedicated addressing and MAC protocol is required [69–72]. Multiple transmitters, therefore, cannot share

		Active Current (mA)	Idle Current (mA)	Sleep Current (nA)
MCU	MSP430 [75]	1	0.7	45
	STM32L[76]	0.45	0.3	140
Tx	Linx-NT [26]	42.5	42.5	1
	CC1101 [77]	27.4	27.4	200
Rx	Linx-NT	22.5	22.5	1
	CC1101	15.4	15.4	200

Table 2: Current consumption of individual modules

the channel without incurring packet losses or increasing energy consumption [73, 74]. In this work, we remove the need for MAC by uniquely identifying the transmitter in each pulse.

Despite its energy efficiency, PPM is not popular in wireless owing to the above challenges. We propose WiChronos, a special case of the more general pulse position modulation for wireless communication and design the modulation to cover a long range and accommodate a large scale. In §6, we will compare the energy efficiency, range, and scalability of M-PPM with WiChronos.

4 WICHRONOS: INTERVAL MODULATION

In the majority of the digital modulation techniques used in wireless networks, data modulates the characteristics of the carrier signal [78]. For e.g., 2-FSK maps bit 0 and bit 1 to two distinct frequencies, transmitting 1 bit per symbol. The total number of symbols per message, therefore, depends on the modulation technique and the message length. Higher-order modulation techniques such as 64-QAM can encode more bits per symbol, but have larger energy per bit, E_b while lower-order modulations such as 2-FSK have lower E_b but an increased number of symbols per message.

A modulation technique that reduces the number of symbols per message without increasing E_b is required to achieve energy efficiency. With this insight, we propose WiChronos, a modulation technique that encodes information in the time interval between two anchor symbols. Fig. 1 illustrates an example with an integer data 678 from a 10-bit sensor. The transmitter sends a predefined preamble and waits for 678 clock cycles and then a predefined postamble. The receiver, with apriori knowledge of the anchor symbols of each transmitter, identifies the sender from the preamble and triggers the corresponding timer to start (or stop) on the reception of the preamble (or postamble). In the absence of any timing errors and prior knowledge of clock rate, the number of clock cycles counted at the receiver is equal to that at the transmitter.

The total number of symbols transmitted on-air and the energy consumed by the RF module depends only on the length of the anchor symbols and is not affected by the length of the sensor output (10-bits in this example). WiChronos hence satisfies the two requirements identified earlier for energy-efficient modulation i.e., (1) Minimum number of symbols, (2) Non-increasing energy per bit E_b. In the rest of this section, we discuss the challenges in achieving the promise of WiChronos and propose solutions to address them.

4.1 Energy Efficiency

A key insight for the energy-efficient design of WiChronos is that the RF module is the bottleneck of a sensor node [28]. Energy consumed by a sensor node is given by $V \cdot I \cdot \delta t$, where V is the voltage, I the average current drawn for a duration δt. For a constant
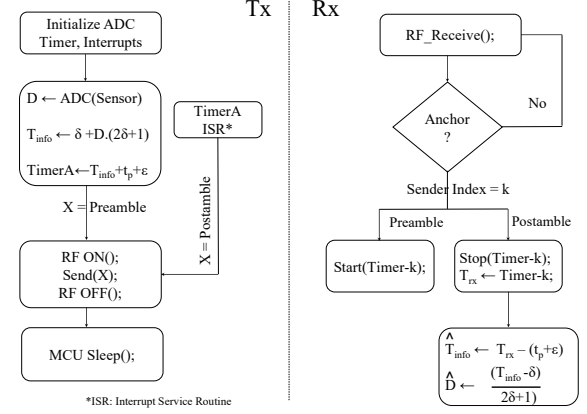
Fig. 2: System implementation flow diagram

V and given δt, the current drawn, which determines the energy consumption can be classified into six categories as,

(1) I_{a-u}: Active - MCU
(2) I_{s-u}: Sleep - MCU
(3) I_{i-rf}: Idle - RF module
(4) I_{s-rf}: Sleep - RF module
(5) I_{r-rf}: Active listen - RF module
(6) I_{t-rf}: Active transmit - RF module

Table 2 enumerates the above currents for selected OTS hardware. The active and sleep currents of MCUs are few *mA* and *μA* respectively, as noted in row 2 of Table 2. I_{t-rf} depends on the transmit power of the RF module and the protocols implemented in the transceiver. The active currents of RF module are on the order of tens of *mA*. Therefore, an energy-efficient transmitter must minimize the amount of time spent in active mode. By encoding information in the time interval between symbols, we reduce the active transmit time of the RF module and the MCU. The energy consumption is further reduced by operating the MCU and the RF module in sleep mode during information transfer (clock count).

Fig. 2 details our implementation in MSP430 FR2355. On reading analog data from the sensor, the transmitter converts it to a digital value (D), maps to clock cycles T_{info} (with redundancy to correct for timing errors) and sets TimerA to T_{info}. The MCU triggers the RF module to send a preamble and then set the RF to sleep. The MCU itself goes to sleep mode, with TimerA running in the background. After T_{info} cycles, TimerA interrupts the MCU to turn on the RF to send postamble. Since T_{info} is the time *difference* between the symbols, the transmitter and receiver clocks need not be synchronized. It is sufficient to use the same clock rate. Since the RF and MCU modules are in sleep mode during data transmission (T_{info}), the overall energy consumption is unaffected by the message length. The energy consumption of data transmission is,

$$E = V \left(I_{a-u} + I_{t-rf} \right) 2t_{anchor} + V \left(I_{s-u} + I_{s-rf} \right) T_{info} \quad (4)$$

where t_{anchor} denotes the duration of anchor symbols. The overall energy consumption is therefore determined by the modulation parameters used to transmit the anchor symbols, the anchor symbol length, and the corresponding current drawn. Optimum anchor symbol length is crucial to achieving the promised energy efficiency.

4.2 Anchor Symbol Design

Predefined preambles and sync words are commonly used in communication systems to indicate the start of a packet, as well as assist the receiver with frame (and/or bit) synchronization [78].
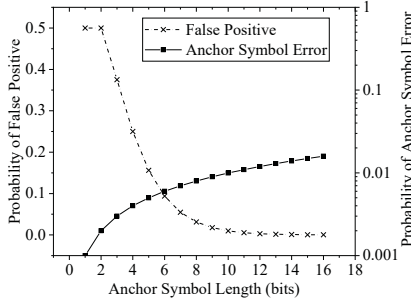
Fig. 3: Anchor symbol length design

Fig. 4: Impact of bandwidth on receiver sensitivity

Fig. 5: Collisions in the network using ALOHA

The anchor symbols play the same role; indicate the start of a message (to start and stop clock counting) and assist the receiver to identify the sender. Since we specifically focus on networks with relaxed data-rate requirements, the anchor symbols are transmitted at the order of few kilobits per second over narrow BW. At such low data-rates, the time and the number of bits required for the Automatic Gain Control (AGC) in the RF front end to settle, is reduced. Further, UNB communication requires much shorter preamble than coded modulations [79]. For example, TI CC1125 [80] uses an AGC design with a 4-bit settling time along with smart carrier sensing to reduce false positives. The lower bound on the anchor symbol length is thus determined by the RF front end and the modulation parameters. In order to differentiate between the start counting and stop counting triggers, each sender is assigned two unique addresses i.e., each sender has a unique preamble and postamble.

We define the optimum anchor symbol length to be the shortest length that enables reliable decoding at the receiver i.e., it must minimize the probability of error in decoding and has a low false-positive rate. For a given modulation, SNR, and the corresponding BER p_b, the probability of symbol error and false-positive are,

$$P_e = \sum_{k=0}^{e} \binom{N}{k} \cdot p_b{}^k q^{N-k}, \qquad P_f = (0.5)^N \sum_{i=0}^{\epsilon} \binom{N}{i} \qquad (5)$$

where e is the maximum number of bit errors that can be tolerated by the receiver for an N-bit anchor symbol. Fig. 3 plots the above probability of symbol error P_e and probability of false positive P_f as a function of anchor symbol length for e=0. P_e increases with symbol length; therefore, shorter anchors are desirable to reduce symbol error while P_f decreases with symbol length. With short symbols, the probability of a random bit pattern from other devices or interference being falsely detected as the anchor is high. We identify the smallest anchor symbol length that renders low P_f and P_e for a given anchor symbol modulation, expected SNR, desired false positive rate, and symbol error rate. In this work, we use BFSK to modulate the anchor symbols with an SNR $\geq$ 10dB, BER of $\leq 10^{-3}$. We choose 10-bit anchor symbol to achieve $P_f \leq 0.01$ and $P_e \leq 0.001$. It must be noted that this shortest anchor symbol length is required to transmit each *pulse* in any variant of PPM. The anchor symbol length calculation is unaffected by the receiver since we leverage the resource asymmetry in infrastructure mode and let the receiver to always be in *listen* mode.

The minimum anchor symbol length is determined by the settling time of the RF module, the probability of false positives, and the probability of symbol error. RF modules with advanced carrier sensing
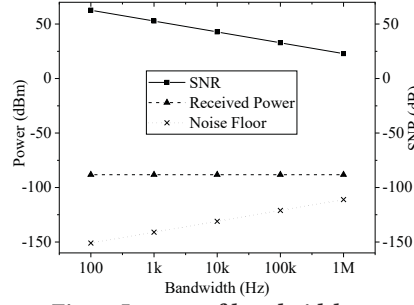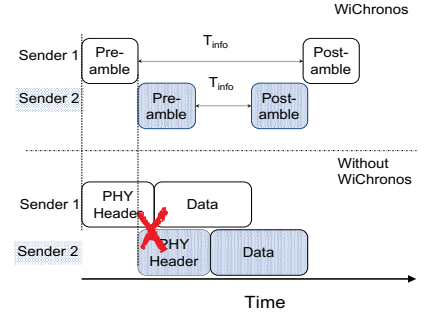
and AGC can further reduce the settling time and false positives, leading to shorter anchor symbols.

4.3 Long-Range Communication

The second challenge identified in this work is achieving long-range within the energy constraints. As discussed in §2, propagation loss is directly proportional to the distance and the frequency of operation. Following the IEEE 802.11ah standard [81], we operate in the sub-GHz spectrum and narrow bandwidth (NB) for long-range. The range also depends on the *receiver sensitivity* (the minimum received power required to demodulate the signal with an acceptable BER), a characteristic of the receiver. For a given propagation channel and frequency of operation, the received power from Equation 2 depends on the transmit power, antenna gains, and the channel. SNR depends on the received power and the noise floor, given by,

$$\text{Noise floor} = -174 + NF + 10 \log_{10} BW. \qquad (6)$$

Here NF is the noise figure (the ratio of input SNR to output SNR at the receiver) and BW is the receiver BW [35]. Fig. 4 shows SNR and NF as a function of BW. For a given received power, the noise floor increases with receiver BW, in turn decreasing the SNR and the receiver sensitivity. NB and UNB modulations are capable of long-range due to their improved receiver sensitivity and SNR from reduced BW. However, decreasing the receiver BW implies reduced transmit BW, leading to an increase in time-on-air and energy consumption. Thus, even in low data-rate applications, wireless systems operate at higher datarates to save battery life. To overcome the impact of narrow BW, existing LPWAN strategies limit the number of messages to reduce the total *time-on-air* [82].

Due to its reduced time-on-air WiChronos can operate in UNB without significantly increasing the energy consumption. The increase in time-on-air from UNB transmission of the anchor symbols is much smaller than that of the entire message (as in other LPWAN techniques). In our evaluation, we modulate the anchor symbols using BFSK in the 902-928MHz spectrum with a BW of 100kHz. RF modules such as TI CC1101 [77], CC1120 [83] can allow us to reach 10s of km with much lower BWs. Operating at the 902-928MHz spectrum also offers the advantage of mitigating multipath reflections and wideband interference. Devices operating in NB and UNB are unaffected by multipath as they experience no inter symbol interference [84, 85]. This is a physical layer phenomenon and we discuss this in our future work as an area of further analysis.

4.4 Medium Access Control

The third challenge identified in this work is co-existence in a large-scale deployment. In spite of the vast research on MAC protocols for large-scale [33, 86], ALOHA-based algorithms are implemented in LPWANs due to its simplicity. ALOHA allows a sender to transmit whenever it has data without any coordination between the senders. The simplicity of ALOHA makes it vulnerable to collisions in large-scale and/or heavy-traffic deployments. A packet collision occurs if one sender begins transmission during an on-going transmission i.e., twice the data transmission period is *vulnerable* to collisions. LPWANs using ALOHA-based MAC protocols suffer from collisions in large-scale networks when the channel is used for transmission more than 20% of the time (on average) [78].

WiChronos (by design) has low time-on-air and leverages the simplicity of ALOHA without getting penalized by collisions. **Data transmission time and time-on-air are different for WiChronos, unlike existing digital modulations.** As shown in Fig. 5,in current systems, the entire transmission is vulnerable to collisions, whereas, in WiChronos, only the anchor symbols are vulnerable, decreasing the probability of collisions. During the *data* transmission of one sender (T_{info}), the other sender can transmit their anchor symbols without affecting the on-going transmissions. We derive the probability of collisions given a node is transmitting a message following the textbook approach used in the analysis of ALOHA [87]. We assume a Poisson arrival process with a cumulative arrival rate of λ. Given a sender started a transmission, the event is a success if no other anchor is sent within $2t_{anchor}$.

$$\Pr(collision) = 1 - \Pr(\text{no other event in } 2T')$$

$$= 1 - e^{-\lambda\, 2\, T'}, \text{where T'} = t_{anchor} \quad (7)$$

Fig. 6 plots the probability of collision for a given node *transmitting a 1-byte message every ten minutes* as a function of the network size. For SigFox, we assume its default overhead of 11 bytes at a datarate of 600bps and the shortest preamble allowed for LoRa with a spreading factor (SF) of 7, code rate 4/5 and 125kHz BW [88], operating in implicit header mode without CRC. We turn off CRC and MAC overheads, as well as ACKs in LoRa for a fair comparison. An arrival rate of 2λ is used in the calculation for WiChronos to account for the two anchor symbols.

With an increase in the number of sensors, the probability of collision for SigFox is the highest among compared technologies, due to its very low data-rate and very high time-on-air. The above parameters for LoRa are chosen for low-power and do not offer long range. For longer range, LoRa recommends higher SF, which will lead to increased time-on-air, thus increasing the probability of collision. The rate of increase of probability of collisions with network scale is slower for WiChronos due to its reduced air-time. *It can achieve energy efficiency without limiting the number of messages and/or the network size..* As shown in Fig. 6, reducing BW increases the probability of collision due to increase in symbol duration. However, this increase in collision is smaller for WiChronos as only the anchor symbol duration contributes to collision as opposed to SigFox or LoRa where the entire payload increases the collision probability. Therefore, we can leverage NB and UNB to improve range without significantly affecting scalability and energy efficiency. In a network of 1000 nodes, the probability of collision

for SigFox and LoRa are 46.3% and 12.75% compared to WiChronos at 1.2% for a BW of 100kHz and 1.8% for 600Hz.

With increasing network size, the anchor symbol length will increase as log function of network size, since each sender is assigned a unique preamble and postamble as the local address. For example, a 2-byte anchor can address a maximum of 2^{11} senders each with a unique 16-bit preamble and postamble ($\frac{2^{16}}{2}$) and 4 initial bits for RF settling ($\frac{2^{15}}{2^4}$). The trade-off between network scale and energy efficiency will determine the anchor symbol length in practice.

5 ACCURACY-THROUGHPUT TRADEOFF

The promise of long battery life and range in a large-scale is achieved at the cost of datarate. WiChronos achieves energy efficiency by offloading the communication burden to timers at the sender and the receiver and hence the data-rate of a link depends on the clock rate at the transceiver. Consider an MCU with a clock rate f_c = 32.768 kHz. If increasing clock cycles each represent a value, a total of 32768 values can be conveyed in 1 s i.e., 15 bits ($log_2(32768)$) can be communicated in one second(plus anchor symbol time). To generalize, the data-rate of a WiChronos link is given by

$$R_b \;=\; \frac{d \cdot f_c}{T_{info}}. \quad (8)$$

T_{info}, the time to transmit a d-bit message is in the range of $[0, 2^d - 1]$. For a uniformly distributed data source where the values of T_{info} are equiprobable, the expected value (average) of $T_{info} = 2^{d-1}$.

The achievable data-rate is lower than that of LPWAN technologies with comparable range. The numerator of data-rate in Equation 8 is a linear function of payload length while the denominator is an exponential function. This is in contrast with existing modulation techniques where the data-rate is a constant that is independent of the payload length. *WiChronos is thus not suitable for applications with high data-rate and low latency demands.*

5.1 Maximizing Data-rate

We present two strategies to improve our data-rate performance: (1) Accurate higher clock rates (2) Efficient Time encoding. As shown in Equation 8, the data-rate of WiChronos is directly proportional to the clock rate f_c at the transmitter. Increasing f_c reduces the time between the anchor symbols for the same number of clock cycles and improve datarate. The accuracy of the clock plays a significant role in improving data-rate. Commercially available ultra low-power crystal oscillators [89], and MEMS clocks [90] offer high accuracy, high rate clocks. We will discuss the impact of clock skew on data-rate and accuracy later in the section.

The second strategy for improving data-rate is aimed at minimizing the average wait time between anchor symbols using apriori knowledge of the source distribution, analogous to source coding. The expected (average) time to transmit a d-bit message is,

$$\mathbf{E} \;=\; \sum_{i=0}^{2^d-1} i \, \Pr(v(i)),$$

where $\Pr(v(i))$ is the probability of sensing a data value $v(i)$. Minimizing **E** will minimize the average time to send a value between 0 and $2^d - 1$, which will maximize the data-rate. This can be reduced to a continuous Knapsack problem [91], where the data values
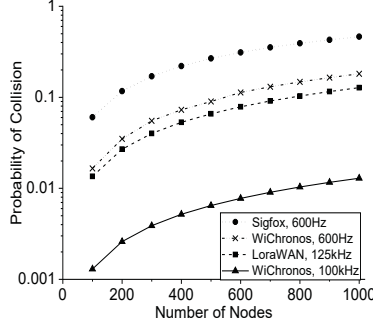
Fig. 6: Probability of collisions

Fig. 7: Timing components of WiChronos sender

must be assigned a time value such that **E** is minimized. It has been proven that the optimum solution for continuous knapsack problem is achieved using greedy algorithm [91] i.e., arrange all possible sensor data in decreasing probability of occurrences and map to increasing time values in $[0, 2^d - 1]$. Mapping the most recurring data to the shortest time, we optimize the data-rate performance.

5.2 Timing Error Correction

The maximum achievable data-rate of a WiChronos link relies on the accuracy of clock rate, processing time, data transmission, and the propagation delay. Fig.7 presents a detailed timeline at a WiChronos transmitter. The currents and the duration listed are specific to the MCU and radio used in our prototype. By default, the radio and the MCU are in sleep mode. The total time to send data includes the radio wake-up time, the anchor symbol transmit time, and the information time. Timing errors in one or more of these components will affect the received T_{info}, leading to bit errors.

We broadly categorize bit errors in received data into the following categories, (1) errors in the anchor symbol, (2) anchor symbol loss, (3) processing and propagation time errors, (4) clock counting error. Existing error detection and correction mechanisms are designed for bit errors and require rethinking for timing errors. We propose a simple error detection mechanism for anchor symbol loss and correction mechanisms for bounded timing errors.

5.2.1 Anchor symbol error and loss. Though we choose the receiver bandwidth and anchor symbol length to minimize BER, there is a non-zero probability for anchor symbol error or loss. Existing coding techniques such as Hamming codes will be used to correct for single bit errors in the anchor symbol. Anchor symbol loss is detected using (1) timeout, (2) stateful receiver. We use the prior knowledge of the maximum payload length and the processing time at the sender to detect anchor loss using *timeout*. For each sender, the timeout value is set to $TO = t_{anchor} + T_{info-max}$, where t_{anchor} is the sum of maximum processing and transmission time to send an anchor symbol and $T_{info-max}$ is the maximum clock cycles mapped to a data. The receiver detects the loss of an anchor symbol whenever the counter exceeds TO. The second detection mechanism maintains the state of the anchor symbol reception for each sender. For every anchor symbol received, the receiver verifies the previous symbol received and the timer value is stored only if a postamble is followed by a preamble. Else, the counter value is discarded, reset and marked as an error, since recurring postambles (or preambles) indicate loss of a preamble(or postamble).
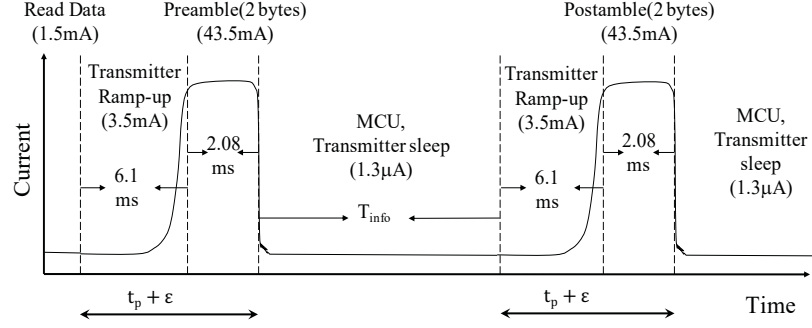
5.2.2 Processing timing error . In Fig.7, let t_p be the average time to send an anchor symbol. t_p is composed of the time to perform the operations in MCU such as ADC, timer setup, serial communication, enter and exit sleep mode, radio wake-up time, modulation, and transmission. Variations in the number of cycles to execute any of these operations can vary t_p in the range $[-\epsilon, +\epsilon]$. We assume that the operations in the MCU are deterministic and do not contribute to ϵ. The radio wake-up time can vary within a bounded range ([26].) We correct for this timing error by triggering the data timer after $t_p + \epsilon$. On reading a sensor data of D, the MCU sets a *transmit counter* for $t_p + \epsilon$ cycles and triggers the radio module to transmit the preamble. At the end of the transmit counter, the MCU and the radio are set to sleep mode for D cycles. By increasing the transmit time from t_p to $t_p + \epsilon$, the transmitter removes the variability in the preamble (and postamble) transmit time. The receiver counts the number of cycles between the preamble and postamble and subtracts $(t_p + \epsilon)$ to obtain T_{info}. We correct for variations in t_p by increasing the overall time to transmit as, $t_{anchor} \geq t_p + \epsilon$. For timing errors bounded by ϵ, the increase in anchor symbol duration from t_p to $t_p + \epsilon$ can achieve 100% error correction.

5.2.3 Clock cycle error. Timing errors due to clock skew at the transceivers can lead to incorrect T_{info} and hence bit errors. We propose a simple error correction mechanism that spreads out the data value (in time) to account for the clock skew. Consider the 32kHz crystal oscillator used in MSP430 FR2355. Though the quartz crystal oscillators have high stability, it has a tolerance of ± 30ppm, resulting in an error of ± 0.9Hz in room temperature [89]i.e., the measured clock cycle can vary by ≈ 1 clock cycle. To correct for this clock counting error, we assign data value D to clock cycles that are separated by 3 i.e., the minimum difference between two adjacent T_{info} transmitted over air is set to three, to correct for variations in the clock cycles measured. To generalize, when using a clock rate with a tolerance of $\pm\delta$, the minimum difference between two transmitted clock cycles is set to δ. Therefore, a sensor data D is mapped to $\delta + D \cdot (2\delta + 1)$. Using the above redundancy in time to correct for clock cycle errors will reduce the effective data-rate since fewer unique clock cycles represent data. Therefore, accurate(low tolerance) clocks are crucial to the design of WiChronos.

5.2.4 Propagation error. The time to receive an anchor symbol includes the propagation delay of the RF signal. At distances of a few *kms*, propagation delays of RF signals traveling at the speed of light are on the order of μseconds. Therefore, changes in propagation delays would also be on the order few μseconds. Error correction mechanism proposed above for clock skew is modified to correct
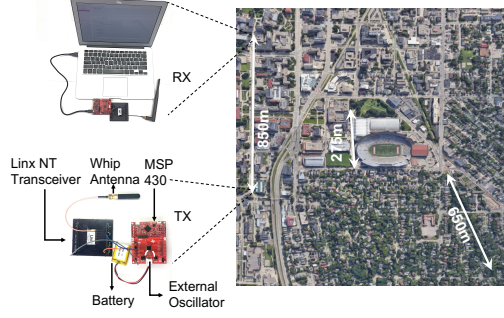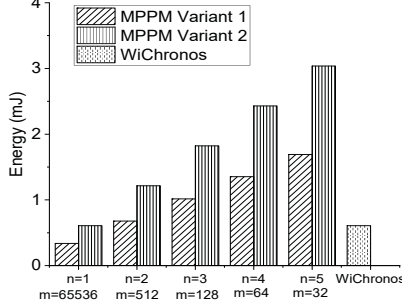
Fig. 8: Experiment locations and set up

Fig. 9: Energy consumption of M-ary PPM and WiChronos

for propagation errors too. A 50% error in propagation delay at a distance of 10 km can lead to an error of ± 0.8 cycles at a clock rate of 32 kHz. Apriori estimate of channel and propagation model is used to encode redundancy. For bounded error in propagation delays, we can achieve 100% error correction by further increasing the minimum difference between adjacent T_{info}. Combining these error detection and correction mechanisms, WiChronos can correct for all bounded errors and detect symbol losses.

6 PERFORMANCE EVALUATION

6.1 Experimental setup

We implement WiChronos using Linx NT [26] as RF module and TI MSP430FR2355 [75] for MCU as shown in Fig.8. Linx-NT has extremely low sleep current(1nA), and a *transparent* mode without protocol overheads. The anchor symbols are transmitted at 9.6kBaud rate using BFSK over 100kHz bandwidth (BW) with a frequency deviation of ± 30kHz [26]. The MCU costs $2.72 and the radio with antenna is $45.8, bringing the overall cost to be < $50. Other less expensive transceivers such as TI CC1101 and CC1125 which cost below $5 can also be used to implement WiChronos. Linx NT is chosen for its simplicity, allowing majority of the parameters to be set through hardware external pins. As part of our future work, we plan to explore various radio modules.

We use a 32.678kHz external crystal oscillator for data transfer (counting) as well as processing (MCU). Since information is encoded in the time difference, absolute clock synchronization is not needed. During system setup, the receiver stores the clock rate and anchor symbol of each transmitter. To understand the impact of timing errors, we estimate the maximum possible timing error analytically, verify it experimentally, and show that it is possible to correct all bounded errors (as explained in §5.2). We compare against LoRa experimentally and present analytical comparison

with SigFox and M-PPM. Easy-to-program, Arduino based integrated LoRa module [92] (RFM69HCW) does not allow for energy management and has low battery life. We implemented an energy management module in SX 1272 [93] operated using MSP430; we reduce its preamble to 6 bytes, remove Cyclic Redundancy Check and MAC headers, disable ACKs, and set to transmit-only mode to minimize its energy consumption and provide fair comparison. Throughout this section, unless otherwise mentioned, we operate LoRa and Linx at 915.37 MHz center frequency. LoRa is implemented at a spreading factor of 7, coding rate 4/5 and BW of 125kHz.

As shown in Fig.8, the sender is powered by a battery and the receiver is always-on. Both the transceivers use the external clock in the MSP and commercially available 1/4-wave whip antennas. Our implementation in MSP shown in Fig.2, circuit design, and hardware setup to recreate our results will be made publicly available[1].

6.2 M-PPM Vs WiChronos

Following our discussion in §3, deploying PPM in a wireless system is challenging. Recently M-ary PPM has been considered for low data rate IOT networks [94]. WiChronos is a special case of the general PPM systems. In this section, we compare M-ary PPM against WiChronos on its energy efficiency, range, and scalability. MPPM encodes a d-bit message to one of 2^d symbols which are represented by **n** pulses in one of the **M** time slots. For example, in Fig.1, a 10-bit message is communicated using n=2 pulses in one of the M=32 slots $[\binom{32}{2} > 2^{10}]$. By transmitting these pulses over NB or UNB, long range can be achieved [94]. In the rest of this section, we assume a 100kHz BW for WiChronos and M-PPM pulses and therefore both the modulations can achieve the same range.

Unlike an optical system, a single pulse needs to be long enough for a wireless receiver to decode. Thus, the pulse length calculation follows that of the anchor symbol. We choose a 1-byte sequence of alternating 1s and 0s as a single pulse since that is the smallest length that can be communicated using Linx NT i.e., the shortest MPPM (and WiChronos) pulse is set to 8 bits. The start of a message is denoted by a 1-byte pulse, followed by the sender address, similar to a WiChronos anchor symbol. Shorter pulse lengths using other RF modules will benefit M-PPM as well as WiChronos. Our implementation of WiChronos uses 2-byte *anchor symbol*, where the first byte is used for synchronization and the second byte to identify the sender. Once an M-PPM receiver decodes the start of a message, it synchronizes the clock and waits for a pulse.The transmitter is in deep sleep mode when it isn't actively transmitting.

We implement the following two variants of MPPM that tradeoff energy and scalability. (1) *Each pulse is 1-byte i.e. the shortest pulse.* The short pulses consume lower energy, at the cost of MAC overheads. Since the receiver cannot differentiate pulses from multiple senders, a dedicated MAC protocol [73] or coding [65, 94] to coordinate transmission is required. (2) *Each transmitter has a unique pulse.* This eliminates MAC overheads but renders each pulse longer, like a WiChronos anchor symbol, trading off energy for scalability. **Energy Consumption:** Fig. 9 compares the energy consumption of WiChronos and the above variants of M-PPM, in transmitting a 2-byte payload. The energy consumption of WiChronos depends only on the length of the anchor symbols, while that of M-PPM
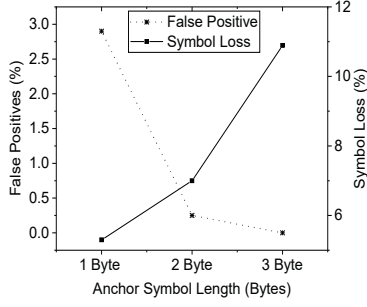
---

[1]https://github.com/Yaman-Sangar/WiChronos

Fig. 10: Experimental verification of anchor symbol length

Fig. 11: Battery life of WiChronos Vs LoRa and SigFox

Fig. 12: Battery life of WiChronos Vs. scale and traffic load

increases linearly with the number of pulses n. For $n = 2$, the energy consumption of M-PPM is the same as WiChronos and requires M=512 slots to transmit a 2-byte message. While increasing n increases energy consumption, it decreases latency.

Scalability: An energy efficient M-PPM system (variant 1) would choose the shortest pulse, which will require MAC overheads and/or additional coding techniques to reduce collision rate. While a scalable M-PPM (variant 2) eliminates MAC overheads, it increases energy per pulse (similar to the anchor symbol of WiChronos), increasing the overall energy consumption and the pulse duration.

Data Rate: The frame duration of M-PPM is fixed for a given payload length i.e., M=32, with 2 pulses can encode 10 bits and always consumes 32 slots. WiChronos on the other hand, has variable message duration between the symbols that depends on the payload. WiChronos leverages lower data rate to achieve energy efficiency.

6.3 Anchor symbol length

In this section, we evaluate the robustness of our anchor symbol length design in §4.2. In our evaluation, we design the length to achieve an SNR $\geq$ 10 dB resulting in a BER of 10^{-3} for BFSK [78]. At BER = 10^{-3}, we determine the optimum symbol length to be 10 bits, with a false positive probability $P_f \leq 0.01$ and symbol error probability $P_e \leq 0.001$ from Fig.3. Linx allows integer multiples of bytes (not bits) and hence we choose a 2-byte anchor symbol. The first byte is a sequence of alternating 1s and 0s to indicate the start of message and the second byte to identify the sender uniquely.

In Fig.10, we experimentally determine P_f and P_e for varying anchor symbol lengths. With increasing anchor symbol length, P_f decreases while P_e increases. At 2-byte anchor symbol, P_f is below 0.01 and P_e below 0.08. The experimental P_e is higher than the expected P_e derived in Equation 5 due to intermittent pedestrian traffic and strong winds. We present the impact of other environmental conditions on the symbol error rate later in the section.

From experiments we infer that the Linx-NT has a higher than average carrier sensing time, resulting in higher false positives. RF modules with smarter carrier sensing can further reduce P_f and hence the anchor symbol length. CC1125 [80] has a 4-bit settling time which can be reduced further by freezing the AGC setting for known input levels. In addition to that, the maximum transmit power of Linx-NT is 13.5 dBm while FCC allows up to 30dBm. An increase in transmit power and decrease in BW can improve SNR, reducing P_e which will allow us to reduce the anchor symbol length further. The presented result is thus an upper bound on the anchor
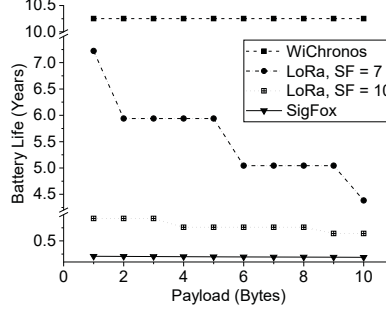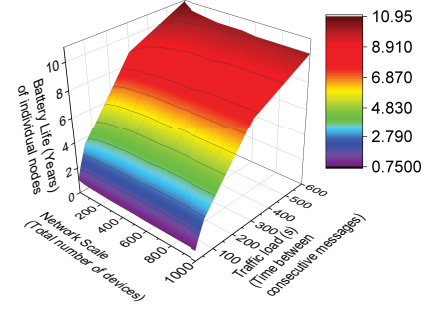
symbol length and offers room for a further decrease in symbol length. *In the rest of our evaluation, we use 2-byte anchor symbols unless stated otherwise.* The receiver determines the preamble using correlation and starts decoding the address byte. A look-up table on the receiver is used to identify the transmitter.

6.4 Energy Efficiency

We evaluate the energy efficiency of WiChronos with 2-byte anchor symbol and compare with LoRa and SigFox. The energy management module we implemented results in longer radio wake-up time. We experimentally measured the average radio wake-up time of Linx to be 4.2ms and that of LoRa $\leq 500\mu s$. In Fig.11, we compare the life of a 250mAh, 3.3V coin-cell battery for varying payload lengths sent every 10 minutes. WiChronos has an impressive 10.25 years life for any payload length as its energy is only a function of the anchor symbol length. LoRa with SF=7 has a battery life of $\approx$ 5 years, but decreases with payload length. LoRa with higher SF used for longer range drastically reduces battery life (7 months at SF=10) while that of SigFox is the lowest at two months.

When transmitting a 2-byte payload, WiChronos reduces energy consumption by **1.7x** compared to LoRa-SF7, **11x** to LoRa-SF10, and **13.55x** to SigFox (BW normalized). The improvement in battery life, which increases with payload length, is due to, 1) reduced air-time 2) non-increasing energy-per-bit E_b. E_b for a WiChronos sender decreases with increasing payload as the overall energy remains constant while the number of bits increases. In classical modulation, E_b is constant and hence their energy increases with payload length. The energy efficiency will be further improved by using modules with smaller sleep currents and faster wake-up time.

The energy efficiency of WiChronos depends only on the length of the anchor symbol and the traffic load. Fig.12 shows the impact of traffic load and network scale on the battery life of a single node. For a given traffic load, battery life of a node decreases with increasing network scale, since the anchor symbol length increases with scale. The anchor symbol length is the sum of minimum decodable pulse (8 bits in this case) and $log_2(NetworkSize) + 1$ to uniquely identify the senders. Similarly, with increasing traffic load, the overall time-on-air increases, in turn decreasing the battery life. At higher traffic loads where a payload is being sent once every 15 or 30 seconds, the battery life reduces considerably as compared to low traffic scenarios. As discussed earlier, WiChronos derives energy savings partly from reducing the time-on-air which increases significantly when the traffic load and/or the scale increases.
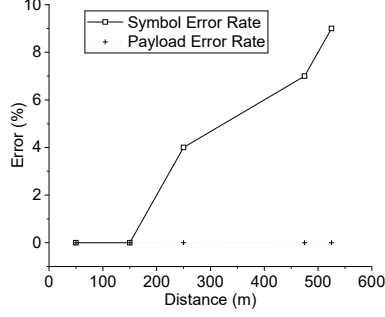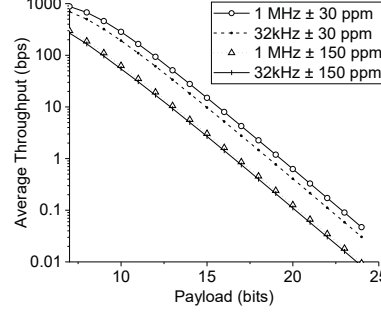
Fig. 13: WiChronos range
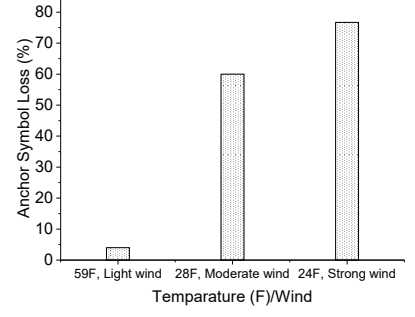

Fig. 14: Datarate performance

Fig. 15: Impact of environmental conditions

6.5 Long Range

The long-range performance of WiChronos depends on the radio module and the modulation parameters used for anchor symbol. In §4.3, we derived the achievable communication range as a function of receiver BW. The maximum achievable range using Linx is limited to 914 meters, due to its reduced transmit power of 13.5 dBm. We verified the feasibility of long-range in indoor and outdoor environments using 1/4-wave whip antenna. Indoor experiments were performed in a 15 m x 10 m office space and along corridors up to 75 m long. Outdoor experiments were performed in streets with car traffic, bike paths with pedestrian traffic, and open fields at varying distances and weather conditions as shown in Fig.8.

Fig.13 plots the percentage of symbol and payload errors at varying distances for a 2-byte payload. The received symbol error remained below 10% at 525 m. At distances up to 850 m, WiChronos implemented on Linx was feasible under line-of-sight conditions. Payload error is the error in decoded data (time). On detecting an anchor symbol loss, the receiver ignores the data. In our experiments, timing errors remained bounded and therefore, payload error is zero, provided the anchor symbols were received correctly. This shows that under bounded errors, proposed mechanisms detect anchor symbol loss and correct timing errors with 100% accuracy.

SNR at the receiver can be improved by increasing the transmit power. RF modules with the maximum allowable Effective Isotropic Radiated Power(EIRP) and lower BW can reach distances of over 10 km [80, 83, 95]. It must be noted that the achievable range of our prototype is constrained by the hardware used here and is not an inherent limitation. Linx was chosen for proof-of-concept because of the ease of hardware programming it offers, simplifying communication between the MCU and the radio. The sleep current of Linx is extremely low which helps keeping the power budget down. Other RF modules such as TI CC1101, CC1125, CC1190 with UNB modulations have been shown to achieve 10s of km, using software programming. Any RF module with a protocol-free mode can be integrated with an MCU to implement WiChronos.

6.6 Error correction and data-rate

We identified four categories of error viz., anchor symbol loss, processing time error, clock skew error, and propagation error. The results presented in the rest of this section incorporate the anchor symbol loss detection. For the other three errors, we evaluate the data-rate performance of WiChronos, the accuracy of received data in the presence of timing error, and the impact of the proposed error correction mechanisms on data-rate. We implement the error correction mechanisms proposed in §5.2 at the transceivers.

6.6.1 Processing time error correction. Fig.7 shows the timeline of WiChronos data transmission, where the duration and currents are specific to the components used in our implementation. As discussed in §5.2, processing time error is corrected by elongating the transmission time t_p to $t_p + \epsilon$. For the system under consideration, $t_p = 196$ cycles and the estimated $t_p + \epsilon = 276$ cycles. At system clock rate of 32.678 kHz, the components of t_p with their corresponding average (A) and maximum (M) clock cycles are, (1) Radio wake-up time + MCU processing (A:137 , M:200) (2) MCU processing (A:8, M:8) (3) 2-byte anchor symbol transmission time at 9.6kBaud (A:51 ,M:68. We estimate the upper bound of each operation to determine ϵ, and validated experimentally. On reading a sensor data, the MCU sets *TimerB* to count up to 276 cycles during radio wake-up and anchor transmission. The effective processing and transmission time is therefore a predetermined constant (276 cycles) and variations within this upper bound does not affect the measured T_{info} at the receiver. The receiver counts T_{info} and subtracts 276 to decode data, achieving 100% accuracy.

6.6.2 Clock skew error. Clock skew directly affects the accuracy of the data received. We evaluate the performance of the two clocks present in MSP430 1) an external crystal oscillator (ECO) 2) an internal Digitally Controlled Oscillator (DCO) and analyse their impact on data-rate. Columns 2-4 in Table 3 show the clock rate and worst case tolerance of these clocks, along with other commercially available low-power clocks. Clock tolerance is an indicator of the accuracy of the clock. For example, with the 32.678 kHz ECO with a tolerance ± 30 parts per million [89] the measured number of clock cycles vary only by ± 1 cycle. We experimentally verified the tolerance levels of the ECO and the DCO by transmitting a predefined value of T_{info} every minute for over a week. Column 5 shows the tolerance determined experimentally for the ECO and DCO. Note that the theoretical tolerance values are an upper bound. Therefore, the clock skew correction proposed in §5.2 uses the tolerance values to determine δ. For the ECO, since $\delta = 1$, a data D is mapped to $T_{info} = 3D + 1$. We correct for clock skew by introducing redundancy, which reduces the effective number of data values D that can be communicated, reducing the data-rate.

Higher tolerance requires higher redundancy for correction, negatively affecting data-rate. Fig.14 plots the achievable data-rate as

Clock Rate	Tolerance ppm	Tolerance cycles	Expt. Tolerance cycles
1 MHz [75]	± 10000	±10000	± 720
32.678 kHz [89]	± 30	± 1	±1
1 MHz [90]	± 50	± 5	Not validated

Table 3: Impact of Clock rate and skew on datarate
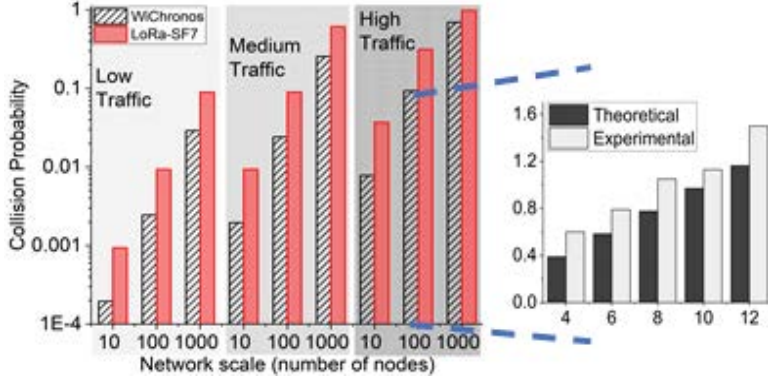
Fig. 16: Collision performance in a multiple access network
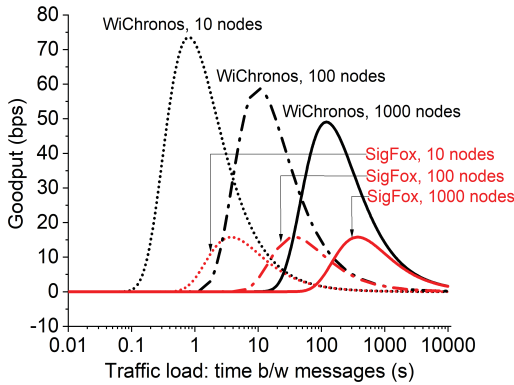

Fig. 17: Goodput Vs load for WiChronos & LoRa

Fig. 18: Goodput Vs load for WiChronos & SigFox

a function of payload for different clocks. When using clock skew error correction, the tolerance has a higher impact on the data-rate than the clock frequency. For a given tolerance, the data-rate of WiChronos with 32kHz and 1MHz are comparable, due to the redundancy introduced for clock skew correction. Accurate clocks are key to the success of WiChronos. Low-power, high accuracy clocks in the order of MHz [90] can be integrated with the MCU to improve the data-rate performance of WiChronos. Note that the data rate decreases with increasing payload length, irrespective of clock tolerance, due to the exponential dependence of information time on the payload. Prior knowledge of source distribution can help with optimum data-time encoding to improve data-rate.

6.7 Multiple Access Control

In Fig. 16, we verify the effectiveness of WiChronos using ALOHA in a large-scale network under varying traffic load. We also experimentally validate the collision probability derived in Equation 7 in a network of 12 senders in heavy traffic scenario. We program the senders to wake up every 16 seconds to communicate a random 2-byte payload. Each sender is assigned a unique preamble and a postamble. On receiving valid bits on the serial interface, the MCU correlates the first byte to detect a packet and decode the second byte to identify the sender uniquely and trigger the corresponding timer. The senders are randomly placed inside a 15 m x 10 m office space. The presented results are averaged over a 2-day period.

We present the probability of collisions in a log scale Y-axis as a function of network scale under varying traffic conditions in Fig.16 The background grey shade darkens as the traffic load increases. We
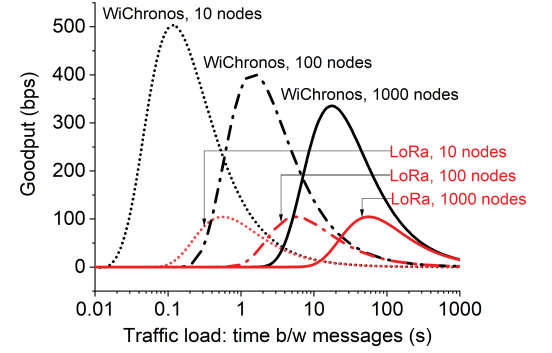
categorize the traffic load as high, medium and low when a 2-byte payload is sent every 15 s, 60 s, and 600 s respectively. As shown in Fig. 16, this probability in a 100 node network with high traffic is 9.1%, 31.3%, and 95% for WiChronos, LoRa with SF-7, and SF-10 respectively. At low traffic, this decreases to 0.24%, 0.93%, and 7.2% for WiChronos, LoRa-SF7, and SF-10 respectively. To compare against SigFox, we use a BW of 600Hz for both WiChronos and SigFox. For low traffic, collision probability is 1.6% and 60.3% for WiChronos and SigFox. Note that the collision probability increases with both network scale and traffic, due to larger volume of data, resulting in higher vulnerability to collisions. This increase in collisions is lower for WiChronos than that of LoRa and SigFox due to its reduced time-on-air. Since the channel is active only for the duration of the anchor symbols, the vulnerable period for collision of WiChronos is smaller for the same bandwidth and payload length.

We also validate the theoretical results with experiments for high-traffic, small-scale network (zoomed-in image). The experimental results reflect the cumulative losses due to collisions, false positives, and anchor symbol losses. On an average, the theoretical collision rate is 75% of the experimental rate; the theoretical results are an approximation for a large scale network and we expect the experimental results to match theoretical for larger networks.

The reduced collision also improves the average network goodput performance (total number of successful data bits in the network in a given duration). We present the average network goodput as a function of traffic load for various network scales in Figs 17 and 18, where each transmitter sends a 2-byte message every *traffic-load* seconds. The above results are BW normalized for fairness, with WiChronos and LoRa using 100kHz and 125kHz respectively in Fig 17 and 600Hz for WiChronos and SigFox in Fig 18. Due to an increase in the volume of data, the goodput increases with traffic initially. However, it reaches an optimal point beyond which, collisions dominate and reduce the number of successful transmissions, inturn reducing goodput. For a given scale, the goodput of WiChronos outperforms LoRa due to its reduced collisions (Fig.16), and they converge at lower traffic. This is because, with reduced traffic load, data volume is low, inversely affecting goodput due to lower utilization of channel capacity. We compare the goodput performance of WiChronos and SigFox in Fig.18. As the scale increases, the increase in collision probability of SigFox is higher than that of WiChronos. Similarly, with reduced traffic load, the decrease in collision is higher for WiChronos, leading to a better goodput.

It must be noted that though WiChronos outperforms LoRa and SigFox in average network goodput, it trades off instantaneous goodput. In a 1000 node network where each node has a 2-byte payload every 10 minutes, the instantaneous goodput of a WiChronos and a LoRa node are 15.0 bps and 517.27 bps respectively. Similarly, with 600 Hz BW, the instantaneous goodput of WiChronos and SigFox are 12.08 bps and 46 bps respectively. WiChronos is therefore best suited for applications with short payloads, where it can deliver low-energy over long-range in a large-scale.

LoRa can leverage the orthogonality of SF to enhance scalability [96]. Lower SF values offer high data rate, and low energy. High SF values help attain a greater range at the cost of data rate. While using different SF could help with scalability, it will also effect the range and battery performance. Another option offered by LoRa and SigFox is to use Frequency Division Multiple Access (FDMA). FDMA can be used in addition to ALOHA to further reduce the collision rate of WiChronos as well. For a given receiver BW, the reduced BW on each sender will increase the collision rate. However, this is only a function of the anchor symbols for WiChronos and the effect will be less pronounced compared to LoRa and SigFox. The decrease in collision rate from the reduced number of devices per channel outweighs the increase (Fig.6) due to lower BW.

6.8 Environmental Conditions

We evaluated WiChronos outdoors under varying weather and traffic conditions. Fig.15 shows the impact of temperature and wind on the anchor symbol error rate at a distance of 250m. SER increases by a factor of 15 at low temperatures and 19 when there are strong winds as well. While this is not a complete analysis, it indicates the strong impact of environmental conditions on anchor symbol loss, and in turn, bit errors at the receiver. We plan to explore the impact of environmental conditions and design antennas and protective casing to reduce the impact in our future work.

7 LIMITATIONS AND FUTURE WORK

WiChronos is the first step towards a low-power, long-range, scalable wireless network for low data-rate LPWANs. There are open research challenges that need further investigation and new research areas stemming from our work such as,

Timing error detection and correction: Existing error correction codes are designed for bit errors. Timing errors in WiChronos can occur due to distance, and channel conditions. Currently, we transmit anchor symbol at low data rates of the order of few kbps, and hence the impact of above conditions on anchor symbol timing is minimal. Error correction mechanisms will be needed for higher anchor symbol rates of 100s of kbps. We proposed a simple error correction mechanism for clock skew that uses the apriori knowledge of the clock tolerance. Smarter, capacity achieving timing error correction can improve the data-rate performance of WiChronos, making it suitable for a wider range of applications.

Data-rate energy tradeoff: WiChronos trades off data rate for energy efficiency. We proposed two strategies to improve the data-rate performance of WiChronos. 1)A greedy algorithm that uses prior knowledge of the source distribution. 2)Information-theoretic and machine learning approaches to learn the source distribution and encode data to clock cycles optimally; also an ongoing work.

Systems research on efficient low-power, high accuracy clocks have the potential to maximize data-rate and minimize energy further. **Anchor symbol loss:** We use timeout to detect anchor loss when messages are shorter than the sensing period. However, when the time between messages decreases, anchor symbol loss can go undetected, leading to inaccurate reception. Further research to handle multiple anchor losses is required to broaden our impact.

Information security and authentication: In its current design, a WiChronos receiver identifies the sender from the anchor symbols and does not offer a mechanism for authentication. An adversary could be listening to the channel to decode data and it is therefore not secure. Encrypting anchor symbol bit pattern can be used to authenticate the sender whereas data security can be achieved by encrypting the data (D) to timing (T_{info})mapping. Simple and efficient security protocols for timing-based communication is a branch of research that is open for further study.

Anchor symbol design: We plan to explore anchor modulations to further decrease the energy consumption and increase the range. We also plan to explore wideband modulation for energy-efficient, scalable, short-range communication scenarios such as on-body sensors. Anchor symbol assigned to each sender is a unique sequence that serves as the sender address. Sequences with high autocorrelation and low cross-correlation properties must used to communicate the addresses reliably. Designing such sequences within the energy budget is challenging and requires further research. In a large scale set up, correlation for identification of senders can be time consuming. We are exploring possible solutions of using chirp spread spectrum (CSS) where each sender is assigned a unique chirp

Medium Access Control: A hybrid of FDMA- or CDMA-based ALOHA can potentially improve the reliability of WiChronos within the energy budget. MAC algorithms leveraging spatial diversity and anchor symbol modulation is a future extension of this work.

Physical layer: WiChronos was implemented using OTS components and we rely on their built-in signal processing for modulation and demodulation, frequency spectrum, AGC timing among other features. Various other transceivers such as TI CC1101 and TI CC1125 offer advantages such as lower AGC settling time, the ability to detect a 4 bit preamble and a much lower active current. Parameters for choosing appropriate hardware may be restricted by the application and requires further study. We are currently working on exploring some of these modules from TI.

8 CONCLUSIONS

We proposed WiChronos, a modulation technique that enables long-range communication in large-scale deployments of energy-constrained sensor nodes. By offloading the communication complexity to timers present in every MCU, we reduce the energy consumption and the cost of each sender. We reduce the time-on-air by minimizing the number of symbols per message, in turn improving the spectral efficiency. The reduced time-on-air enables an ALOHA-based MAC protocol to accommodate a large-scale network without significantly affecting the collision performance. We propose error detection and correction mechanisms for timing induced bit errors for bounded errors. Using off-the-shelf RF modules and MCUs, we prototype and evaluated the energy, range, and scale performance experimentally in indoor and outdoor scenarios.

REFERENCES

[1] Mare Srbinovska, Cvetan Gavrovski, Vladimir Dimcev, Aleksandra Krkoleva, and Vesna Borozan. Environmental parameters monitoring in precision agriculture using wireless sensor networks. *Journal of cleaner production*, 88:297–307, 2015.

[2] JA López Riquelme, Fulgencio Soto, J Suardíaz, P Sánchez, Andres Iborra, and JA Vera. Wireless sensor networks for precision horticulture in southern spain. *Computers and electronics in agriculture*, 68(1):25–35, 2009.

[3] Hanwook Chung, Jingjie Li, Younghyun Kim, and Christopher Y Choi. Continuous and wireless skin contact and ear implant temperature measurements and relations to the core body temperature of heat stressed dairy cows. In *10th International Livestock Environment Symposium (ILES X)*, page 1. American Society of Agricultural and Biological Engineers, 2018.

[4] Haider Jawad, Rosdiadee Nordin, Sadik Gharghan, Aqeel Jawad, and Mahamod Ismail. Energy-efficient wireless sensor networks for precision agriculture: A review. *Sensors*, 17(8):1781, 2017.

[5] National Soil Moisture Network. http://nationalsoilmoisture.com/.

[6] National Ecological Observatory Network. https://www.neonscience.org/.

[7] Decagon 10HS Soil Moisture Sensor. http://www.labcell.com/environmental/soil-moisture-sensors/10hs-soil-moisture-sensor.

[8] EC5 Soil Moisture Sensor. http://www.labcell.com/environmental/soil-moisture-sensors/ec5-soil-moisture-sensor.

[9] TEROS 12: Avanced soil moisture sensing. https://www.metergroup.com/environment/products/teros-12/.

[10] Shahin Farahani. *ZigBee wireless networks and transceivers*. Newnes, 2011.

[11] Carles Gomez, Joaquim Oller, and Josep Paradells. Overview and evaluation of bluetooth low energy: An emerging low-power wireless technology. *Sensors*, 12(9):11734–11753, 2012.

[12] Colby Boyer and Sumit Roy. âĂŤinvited paperâĂŤbackscatter communication and rfid: Coding, energy, and mimo analysis. *IEEE Transactions on Communications*, 62(3):770–785, 2014.

[13] Vincent Liu, Aaron Parks, Vamsi Talla, Shyamnath Gollakota, David Wetherall, and Joshua R Smith. Ambient backscatter: wireless communication out of thin air. In *ACM SIGCOMM Computer Communication Review*, volume 43, pages 39–50. ACM, 2013.

[14] Yao Peng, Longfei Shangguan, Yue Hu, Yujie Qian, Xianshang Lin, Xiaojiang Chen, Dingyi Fang, and Kyle Jamieson. Plora: A passive long-range data network from ambient lora transmissions. In *Proceedings of the 2018 Conference of the ACM Special Interest Group on Data Communication*. ACM, 2018.

[15] Vamsi Talla, Mehrdad Hessar, Bryce Kellogg, Ali Najafi, Joshua R Smith, and Shyamnath Gollakota. Lora backscatter: Enabling the vision of ubiquitous connectivity. *Proceedings of the ACM on Interactive, Mobile, Wearable and Ubiquitous Technologies*, 1(3):105, 2017.

[16] Thomas M Cover and Joy A Thomas. *Elements of information theory*. John Wiley & Sons, 2012.

[17] Deepak Ganesan Pan Hu, Pengyu Zhang. Laissez-faire : Fully asymmetric backscatter communication. In *Proceedings of the 2015 ACM Conference on Special Interest Group on Data Communication*, pages 255–267. ACM, 2015.

[18] V. Pillai, H. Heinrich, D. Dieska, P. V. Nikitin, R. Martinez, and K. V. S. Rao. An ultra-low-power long range battery/passive rfid tag for uhf and microwave bands with a current consumption of 700 na at 1.5 v. *IEEE Transactions on Circuits and Systems I: Regular Papers*, 54(7):1500–1512, 2007.

[19] LoRa. https://www.semtech.com/lora.

[20] SigFox. https://www.sigfox.com/en/sigfox-iot-radio-technology.

[21] NB-IoT. https://www.gsma.com/iot/narrow-band-internet-of-things-nb-iot/.

[22] Juha Petäjäjärvi, Konstantin Mikhaylov, Matti Hämäläinen, and Jari Iinatti. Evaluation of lora lpwan technology for remote health and wellbeing monitoring. In *2016 10th International Symposium on Medical Information and Communication Technology (ISMICT)*, pages 1–5. IEEE, 2016.

[23] Ruslan Kirichek and Vyacheslav Kulik. Long-range data transmission on flying ubiquitous sensor networks by using lpwan protocols. In *International Conference on Distributed Computer and Communication Networks*. Springer, 2016.

[24] William Hart Hayt, John A Buck, et al. *Engineering electromagnetics*, volume 6. McGraw-Hill New York, 1981.

[25] MSP 430 user guide. http://www.ti.com/lit/ug/slau445i/slau445i.pdf.

[26] Linx NT Series Transceiver User Guide. https://linxtechnologies.com/wp/wp-content/uploads/trm-fff-nt.pdf.

[27] Gregory J Pottie and William J Kaiser. Wireless integrated network sensors. *Communications of the ACM*, 43(5):51–58, 2000.

[28] Vijay Raghunathan, Curt Schurgers, Sung Park, and Mani B Srivastava. Energy-aware wireless microsensor networks. *IEEE Signal processing magazine*, 2002.

[29] Giuseppe Anastasi, Marco Conti, Mario Di Francesco, and Andrea Passarella. Energy conservation in wireless sensor networks: A survey. *Ad hoc networks*, 7(3):537–568, 2009.

[30] Tifenn Rault, Abdelmadjid Bouabdallah, and Yacine Challal. Energy efficiency in wireless sensor networks: A top-down survey. *Computer Networks*, 2014.

[31] Ridha Soua and Pascale Minet. A survey on energy efficient techniques in wireless sensor networks. In *2011 4th Joint IFIP Wireless and Mobile Networking Conference (WMNC 2011)*, pages 1–9. IEEE, 2011.

[32] Gang Lu, Bhaskar Krishnamachari, and Cauligi S Raghavendra. An adaptive energy-efficient and low-latency mac for data gathering in wireless sensor networks. In *18th International Parallel and Distributed Processing Symposium, 2004. Proceedings.*, page 224. IEEE, 2004.

[33] Ilker Demirkol, Cem Ersoy, and Fatih Alagoz. Mac protocols for wireless sensor networks: a survey. *IEEE Communications Magazine*, 44(4):115–121, 2006.

[34] Wei Ye, John Heidemann, and Deborah Estrin. Medium access control with coordinated adaptive sleeping for wireless sensor networks. *IEEE/ACM Transactions on Networking (ToN)*, 12(3):493–506, 2004.

[35] Andrea Goldsmith. *Wireless communications*. Cambridge university press, 2005.

[36] Injong Rhee, Ajit Warrier, Mahesh Aia, Jeongki Min, and Mihail L Sichitiu. Z-mac: a hybrid mac for wireless sensor networks. *IEEE/ACM Transactions on Networking (TON)*, 16(3):511–524, 2008.

[37] Naoto Kimura and Shahram Latifi. A survey on data compression in wireless sensor networks. In *International Conference on Information Technology: Coding and Computing (ITCC'05)-Volume II*, volume 2, pages 8–13. IEEE, 2005.

[38] David Chu, Amol Deshpande, Joseph M Hellerstein, and Wei Hong. Approximate data collection in sensor networks using probabilistic models. In *22nd International Conference on Data Engineering (ICDE'06)*, pages 48–48. IEEE, 2006.

[39] Bhargav Kanagal and Amol Deshpande. Online filtering, smoothing and probabilistic modeling of streaming data. In *2008 IEEE 24th International Conference on Data Engineering*, pages 1160–1169. IEEE, 2008.

[40] Aria Nosratinia, Todd E Hunter, and Ahmadreza Hedayat. Cooperative communication in wireless networks. *IEEE communications Magazine*, 2004.

[41] Zhong Zhou, Shengli Zhou, Shuguang Cui, and Jun-Hong Cui. Energy-efficient cooperative communication in a clustered wireless sensor network. *IEEE Transactions on Vehicular Technology*, 2008.

[42] Paolo Casari, Alessia Marcucci, Michele Nati, Chiara Petrioli, and Michele Zorzi. A detailed simulation study of geographic random forwarding (geraf) in wireless sensor networks. In *MILCOM 2005-2005 IEEE Military Communications Conference*, pages 59–68. IEEE, 2005.

[43] Jamal N Al-Karaki and Ahmed E Kamal. Routing techniques in wireless sensor networks: a survey. *IEEE wireless communications*, 11(6):6–28, 2004.

[44] Vamsi Paruchuri, Shivakumar Basavaraju, Arjan Durresi, Rajgopal Kannan, and S Sitharama Iyengar. Random asynchronous wakeup protocol for sensor networks. In *First International Conference on Broadband Networks*. IEEE, 2004.

[45] IEEE Standard 802.15.4. https://standards.ieee.org/standard/802_15_8-2017.html.

[46] Benjie Chen, Kyle Jamieson, Hari Balakrishnan, and Robert Morris. Span: An energy-efficient coordination algorithm for topology maintenance in ad hoc wireless networks. *Wireless networks*, 8(5):481–494, 2002.

[47] M. S. Trotter and G. D. Durgin. Survey of range improvement of commercial rfid tags with power optimized waveforms. In *2010 IEEE International Conference on RFID (IEEE RFID 2010)*, pages 195–202. IEEE, 2010.

[48] Mehran Abolhasan, Tadeusz Wysocki, and Eryk Dutkiewicz. A review of routing protocols for mobile ad hoc networks. *Ad hoc networks*, 2(1):1–22, 2004.

[49] Vikram Iyer, Rajalakshmi Nandakumar, Anran Wang, Sawyer Fuller, and Shyamnath Gollakota. Living iot: A flying wireless platform on live insects. *arXiv preprint arXiv:1812.09419*, 2018.

[50] Evşen Yanmaz, Saeed Yahyanejad, Bernhard Rinner, Hermann Hellwagner, and Christian Bettstetter. Drone networks: Communications, coordination, and sensing. *Ad Hoc Networks*, 68:1–15, 2018.

[51] Rapeepat Ratasuk, Nitin Mangalvedhe, Yanji Zhang, Michel Robert, and Jussi-Pekka Koskinen. Overview of narrowband iot in lte rel-13. In *2016 IEEE conference on standards for communications and networking (CSCN)*, pages 1–7. IEEE, 2016.

[52] Zigbee 3.0. https://www.nxp.com/products/wireless/zigbee/zigbee/zigbee-3.0:ZIGBEE-3-0.

[53] Venkat Anantharam and Sergio Verdu. Bits through queues. *IEEE Transactions on Information Theory*, 42(1):4–18, 1996.

[54] Anand S Bedekar and Murat Azizoglu. The information-theoretic capacity of discrete-time queues. *IEEE Transactions on Information Theory*, 1998.

[55] Rajesh Sundaresan and Sergio Verdú. Robust decoding for timing channels. *IEEE Transactions on information Theory*, 46(2):405–419, 2000.

[56] Rajesh Sundaresan and Sergio Verdú. Capacity of queues via point-process channels. *IEEE/ACM Transactions on Networking (TON)*, 14(SI):2697–2709, 2006.

[57] Balaji Prabhakar and Robert Gallager. Entropy and the timing capacity of discrete queues. *IEEE Transactions on Information Theory*, 49(2):357–370, 2003.

[58] Sarah H Sellke, C-C Wang, Saurabh Bagchi, and Ness Shroff. Tcp/ip timing channels: Theory to implementation. In *IEEE INFOCOM 2009*. IEEE, 2009.

[59] Pandurang Kamat, Wenyuan Xu, Wade Trappe, and Yanyong Zhang. Temporal privacy in wireless sensor networks: Theory and practice. *ACM Transactions on Sensor Networks (TOSN)*, 5(4):28, 2009.

[60] Wenyuan Xu, Wade Trappe, and Yanyong Zhang. Anti-jamming timing channels for wireless networks. In *Proceedings of the first ACM conference on Wireless network security*, pages 203–213. ACM, 2008.

[61] Yujie Zhu and Raghupathy Sivakumar. Challenges: communication through silence in wireless sensor networks. In *Proceedings of the 11th annual international conference on Mobile computing and networking*, pages 140–147. ACM, 2005.

[62] Da-shan Shiu and Joseph M Kahn. Differential pulse-position modulation for power-efficient optical communication. *IEEE transactions on communications*, 47(8):1201–1210, 1999.

[63] Zabih Ghassemlooy, AR Hayes, NL Seed, and ED Kaluarachchi. Digital pulse interval modulation for optical communications. *IEEE Communications Magazine*, 36(12):95–99, 1998.

[64] Hisayoshi Sugiyama and Kiyoshi Nosu. Mppm: A method for improving the band-utilization efficiency in optical ppm. *Journal of Lightwave Technology*, 7(3):465–472, 1989.

[65] Hyuncheol Park and J. R. Barry. Trellis-coded multiple-pulse-position modulation for wireless infrared communications. *IEEE Transactions on Communications*, 52(4):643–651, April 2004.

[66] Hyuncheol Park and J. R. Barry. Modulation analysis for wireless infrared communications. In *Proceedings IEEE International Conference on Communications ICC '95*, volume 2, pages 1182–1186 vol.2, June 1995.

[67] Li Zhao and A. M. Haimovich. Multi-user capacity of m-ary ppm ultra-wideband communications. In *2002 IEEE Conference on Ultra Wideband Systems and Technologies (IEEE Cat. No.02EX580)*, pages 175–179, May 2002.

[68] Li Zhao and A. M. Haimovich. Capacity of m-ary ppm ultra-wideband communications over awgn channels. In *IEEE Vehicular Technology Conference*, 2001.

[69] Zhi Zhang, Zhonghai Lu, Qiang Chen, Xiaolang Yan, and Li-Rong Zheng. Code division multiple access/pulse position modulation ultra-wideband radio frequency identification for internet of things: concept and analysis. *International Journal of Communication Systems*, 25(9):1103–1121, 2012.

[70] Francesca Cuomo and C Martello. Mac principles for an ultra wide band wireless access. In *IEEE Global Telecommunications Conference (Cat. No. 01CH37270)*, 2001.

[71] Xuemin Shen, Weihua Zhuang, Hai Jiang, and Jun Cai. Medium access control in ultra-wideband wireless networks. *IEEE Transactions on Vehicular Technology*, 54(5):1663–1677, 2005.

[72] Dong Sam Ha and Patrick R Schaumont. Replacing cryptography with ultra wideband modulation in secure rfid. In *2007 IEEE International Conference on RFID*.

[73] Z. Lin and P. Wei. Pulse position modulation time hopping ultra wideband sharing signal for radar and communication system. In *2006 CIE International Conference on Radar*, pages 1–4, Oct 2006.

[74] R. Scholtz. Multiple access with time-hopping impulse modulation. In *Proceedings of IEEE Military Communications Conference*, 1993.

[75] MSP 430 FR2355. http://www.ti.com/product/MSP430FR2353.

[76] STM32L151x6. https://www.st.com/resource/en/datasheet/cd00277537.pdf.

[77] TI CC1101 datasheet. www.ti.com/lit/gpn/cc1101.

[78] Theodore S Rappaport et al. *Wireless communications: principles and practice*, volume 2. prentice hall PTR New Jersey, 1996.

[79] Long-range RF communication:. http://www.ti.com/lit/wp/swry006/swry006.pdf.

[80] TI CC1125 datasheet. http://www.ti.com/lit/ds/symlink/cc1125.pdf.

[81] Matthew Gast. *802.11 wireless networks: the definitive guide.* " O'Reilly Media, Inc.", 2005.

[82] Kais Mekki, Eddy Bajic, Frederic Chaxel, and Fernand Meyer. A comparative study of lpwan technologies for large-scale iot deployment. *ICT Express*, 2019.

[83] CC1120 High-Performance RF Transceiver for Narrowband Systems. http://www.ti.com/lit/ds/symlink/cc1120.pdf.

[84] Chuhan Gao, Mehrdad Hessar, Krishna Chintalapudi, and Bodhi Priyantha. Blind distributed mu-mimo for iot networking over vhf narrowband spectrum. In *International Conference on Mobile Computing and Networking*. ACM, 2019.

[85] Cory Beard and William Stallings. *Wireless Communication Networks and Systems*. Pearson Education, 2015.

[86] Pei Huang, Li Xiao, Soroor Soltani, Matt W Mutka, and Ning Xi. The evolution of mac protocols in wireless sensor networks: A survey. *IEEE communications surveys & tutorials*, 15(1):101–120, 2013.

[87] James F. Kurose and Keith W. Ross. *Computer Networking: A Top-Down Approach (6th Edition)*. Pearson, 6th edition, 2012.

[88] LoRa Airtime Calculator. https://www.loratools.nl/#/airtime,.

[89] 32 kHz crystal oscillator.

[90] Ultra-Small Low Power, Low-Jitter, 1 Hz to 2.5 MHz Oscillator. https://www.sitime.com/products/1-hz-2-mhz-oscillatorstcxo/sit1579.

[91] Bernhard Korte, Jens Vygen, B Korte, and J Vygen. *Combinatorial optimization*, volume 2. Springer, 2012.

[92] Adafruit Feather 32u4 Radio . https://www.adafruit.com/product/3076.

[93] LoRa. https://www.semtech.com/products/wireless-rf/lora-transceivers/sx1272.

[94] Y. Chen, N. Chiotellis, L. Chuo, C. Pfeiffer, Y. Shi, R. G. Dreslinski, A. Grbic, T. Mudge, D. D. Wentzloff, D. Blaauw, and H. S. Kim. Energy-autonomous wireless communication for millimeter-scale internet-of-things sensor nodes. *IEEE Journal on Selected Areas in Communications*, 34(12):3962–3977, Dec 2016.

[95] FCC Regulations. https://transition.fcc.gov/Bureaus/Engineering_Technology/Documents/bulletins/oet63/oet63rev.pdf.

[96] Floris; Moerman Ingrid; Hoebeke Jeroen Haxhibeqiri, Jetmir; Van den Abeele. Lora scalability: A simulation model based on interference measurements. *Sensors*, 16(6).